Effects of Doping Profile on GaAs Double-Drift IMPATT Diodes at 33 and 44 GHz Using the Energy-Momentum Transport Model

MOUSTAFA A. EL-GABALY, SENIOR MEMBER, IEEE, RICHARD K. MAINS, MEMBER, IEEE, AND GEORGE I. HADDAD, FELLOW, IEEE

Abstract—**Experimentally determined doping profiles for double-read GaAs IMPATT diodes operating at 33 [1], [2] and 44 GHz [3] are used as starting points for a computer optimization. A computer simulation including energy and momentum relaxation effects [4] was used to simulate these devices as the lengths of the drift regions and the integrated charge in the doping spikes were varied. The effects of these doping profile variations on diode performance are presented.**

I. INTRODUCTION

IT WAS FOUND experimentally [5] that the drift lengths for millimeter-wave GaAs IMPATT's should be shorter than the values predicted by a conventional drift-diffusion analysis which uses the static velocity-field characteristic for GaAs. Theoretical studies with a simulation using the energy-momentum transport model [4] identified the primary mechanisms responsible for this behavior to be velocity undershoot and delay of the avalanche process due to energy relaxation. Since the energy-momentum simulation has so far yielded very good agreement with experimental results for millimeter-wave GaAs IMPATT's [6], this model has been used to study the effects of varying certain parameters in the doping profiles in order to establish better design criteria for GaAs IMPATT's. The effects of varying the electron and hole drift lengths are studied using this simulation. Also, the integrated charge in the doping spikes located at the edges of the high-field region in double-read structures is varied. This has the effect of varying the electric field level in the drift regions. *Increasing the electric field in the drift regions allows a greater V_{RF}/V_{dc} voltage modulation, which increases the device efficiency; however, if the field is too large avalanching can occur in the drift regions, which reduces the efficiency. Therefore, a compromise between these two effects must be reached in order to maximize the device efficiency.*

Manuscript received December 9, 1983; revised April 2, 1984. This work was supported by the Air Force Systems Command, Avionics Laboratory, Wright-Patterson Air Force Base, OH, under Contract F33615-81-K-1429.

The authors are with the Solid-State Electronics Laboratory, Department of Electrical and Computer Engineering, University of Michigan, Ann Arbor, MI 48109.

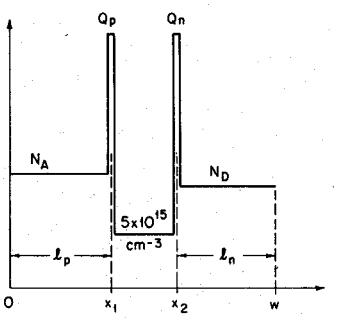

Fig. 1. Double-read doping configuration used for all the simulations. The p-n junction is midway between x_1 and x_2.

II. RESULTS AT 33 GHz

Fig. 1 shows the GaAs IMPATT doping configuration used for all the simulations. This is a double-read structure with the p-n junction midway between x_1 and x_2. N_A and N_D are the doping levels in the p and n drift regions, respectively. Q_p and Q_n are the integrated charges in units of cm^{-2} of the narrow spikes at the edges of the high-field region which serve to bring the electric field down to the desired level in the drift regions.

Table I presents the optimum large-signal results obtained at $f = 33.7$ GHz, $T = 500$ K, and $J_{dc} \approx 5.8$ kA/cm^2. These results are optimum in the sense that the device efficiency η in Table I is the maximum that was obtained. Case 1 was the starting profile obtained from [1], [2], except that the doping spikes Q_n and Q_p were modified from those given in [1] in order to match the experimental operating voltage. In cases 2 and 3, the length of the n drift region is progressively shortened from 0.42 to 0.26 μm, and it is observed that the drive efficiency increases from 24.85 to 27.0 percent. A further decrease of l_n did not increase the efficiency above 27.0 percent. In cases 4 and 5, l_n is held at 0.25 μm and the p drift length l_p is varied about the starting value of 0.42 μm; it is seen that the best efficiency is obtained for the original length of 0.42 μm. After the lengths were optimized, the doping spikes Q_p and Q_n were reduced in order to increase the electric field in the drift regions. The best efficiency of $\eta = 29.16$ percent was then obtained for case 6.

0018-9480/84/1353$01.00 ©1984 IEEE

TABLE I
OPTIMUM LARGE-SIGNAL RESULTS AT 33.7 GHZ FOR DIFFERENT DOPING PROFILE PARAMETERS USING THE ENERGY-MOMENTUM SIMULATION
$N_A = 3.0\times10^{16}\ \text{cm}^{-3}$, $N_D = 7.0\times10^{15}\ \text{cm}^{-3}$, $T = 500$ K

Case No.	ℓ_p (μm)	ℓ_n (μm)	w (μm)	Q_p (10^{12} cm^{-2})	Q_n (10^{12} cm^{-2})	V_{RF} (V)	V_{op} (V)	J_{dc} (kA/cm^2)	η (%)	Y_D (s/cm^2)	P_{RF} (W/cm^2)	P_{RF} (1 Ω)(W)	P_{diss} (1 Ω)(W)
1	0.42	0.42	1.0	2.85	3.0	15.0	24.43	5.94	24.85	-320.7 +j2153	3.606 x 10^4	2.44	7.38
2	0.42	0.32	0.9	2.85	3.0	14.5	23.41	5.77	26.26	-337.5 +j2390	3.547 x 10^4	2.05	5.77
3	0.42	0.26	0.84	2.85	3.0	14.0	22.96	5.85	27.0	-370.5 +j2549	3.626 x 10^4	2.02	5.48
4	0.33	0.25	0.74	2.85	3.0	13.0	21.78	5.90	26.5	-403.6 +j2803	3.411 x 10^4	1.72	4.75
5	0.53	0.25	0.94	2.85	3.0	12.5	23.7	5.75	23.07	-402.7 +j2308	3.144 x 10^4	2.31	7.69
6	0.43	0.25	0.84	1.84	1.84	18.0	25.74	5.94	29.16	-275.2 +j2533	4.458 x 10^4	1.89	4.59

Fig. 2(a) shows the dc solution for the original structure corresponding to case 1 in Table I, and Fig. 2(b) shows the device terminal waveforms for the most efficient large-signal solution obtained for this case (the injected current is the spatial integral of the avalanche generation within the device, and the lower curve labeled "current density" is the total diode terminal current minus the displacement component, or the "induced" current). For comparison, Fig. 3(a) shows the dc solution for case 6 of Table I, and Fig. 3(b) shows the most efficient large-signal solution obtained. In Fig. 2(a), the electric field at the edges of the high-field regions is approximately 2×10^5 V/cm, whereas higher efficiency was obtained with this field raised to approximately 2.7×10^5 V/cm by lowering Q_n and Q_p as shown in Fig. 3(a).

The dip in the induced current waveforms in Figs. 2(b) and 3(b) at 270° in the cycle and the subsequent peak beyond 270° are caused principally by velocity modulation of holes for these structures. Fig. 4(a) shows the electron and hole velocities at 270° in the cycle of Fig. 3(b). Due to the higher doping in the p-region, the electric field is brought down to a low value, whereas on the more lightly doped n side the field remains high due to space-charge effects. It is seen in Fig. 4(a) that the hole velocity is significantly below the saturated velocity of 5.2×10^6 cm/s. In Fig. 4(b) the velocities at 313.2° in the cycle are shown; the hole velocity has now recovered to nearly the saturated value due to the rising electric field. Shortening the n side allows more electrons to be extracted by the beginning of the next cycle, reducing the current between 0° and 90° in Fig. 3(b).

Table II shows large-signal simulation results obtained for the starting structure (case 1 of Table I) at 33.7 GHz as a function of dc bias current density. For each current density, P_{RF} is the RF output power that would be obtained if the device area were chosen so that the diode is matched to 1-Ω circuit resistance, assuming no device or circuit parasitic resistance. The parameter θ_R in Table II is the thermal resistance that would be required to operate the diode under CW conditions at 225°C above the ambient temperature for this case. *If the diode can be matched to*

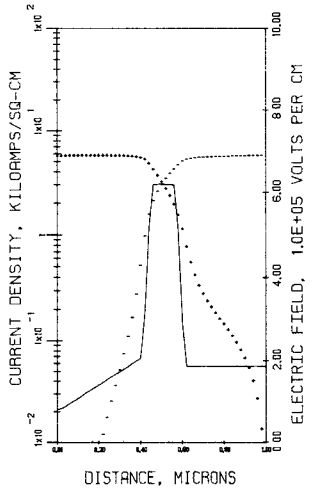

(a)

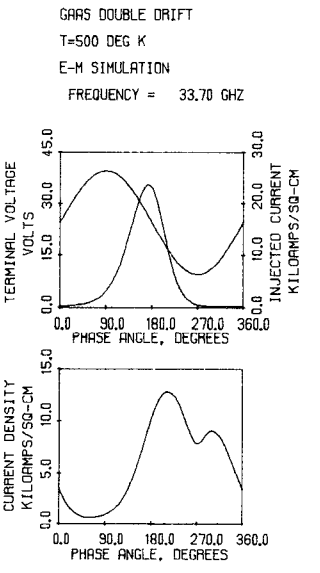

(b)

Fig. 2. (a) DC solution for case 1 of Table I ($T = 500$ K, $J_{dc} = 5.8$ kA/cm^2, $V_{dc} = 23.92$ V) and (b) most efficient large-signal solution for this case ($f = 33.7$ GHz, $V_{RF} = 15.0$ V, $J_{dc} = 5.94$ kA/cm^2, $T = 500$ K, $\eta = 24.85$ percent).

TABLE II
LARGE-SIGNAL RESULTS FOR STRUCTURE 1 OF TABLE I
$f = 33.7$ GHz, $T = 500$ K, $R_c = 1\ \Omega$ matching

J_{dc} (kA/cm^2)	$-G_D$ (s/cm^2)	B_D (s/cm^2)	D (inch)	V_{RF} (V)	V_{op} (V)	η (%)	P_{RF} (W)	P_{diss} (W)	θ_R (°C/W)
5.92	363.7	2131	0.00392	14.0	24.86	24.2	2.77	8.68	25.9
6.94	412.2	2069	0.00427	14.0	24.74	23.5	4.17	11.7	19.2
8.10	458.7	1996	0.00464	14.0	24.60	22.5	5.13	16.7	13.5
10.0	478.6	1861	0.00506	14.0	23.80	19.7	6.08	24.7	9.10
12.0	400.0	1719	0.005	14.0	22.65	14.4	5.03	29.9	7.53

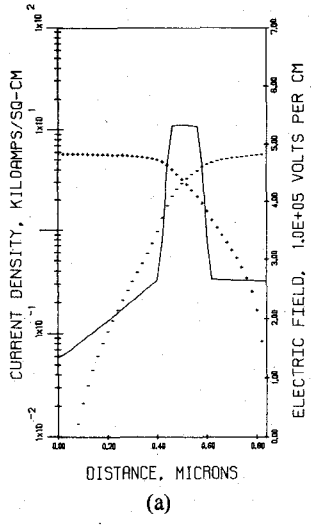

(a)

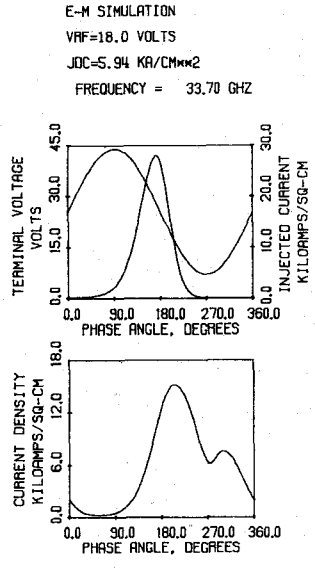

(b)

Fig. 3. (a) DC solution for case 6 of Table I ($T = 500$ K, $J_{dc} = 5.8$ kA/cm^2, $V_{dc} = 24.1$ V) and (b) most efficient large-signal solution for this case ($f = 33.7$ GHz, $V_{RF} = 18.0$ V, $J_{dc} = 5.94$ kA/cm^2, $T = 500$ K, $\eta = 29.16$ percent).

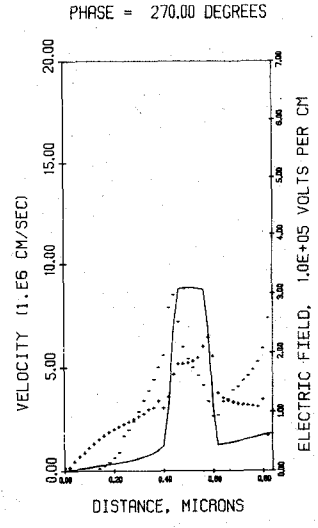

(a)

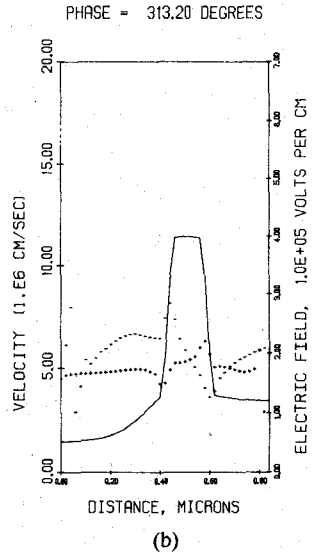

(b)

Fig. 4. (a) Electron and hole velocities at 270° in the cycle of Fig. 3(b) and (b) velocities at 313.2° in the cycle.

a circuit resistance less than 1 Ω, *proportionately more power can be extracted than the values given in Table II.* However if circuit parasitic resistance is present, denoted by R_s, the power actually delivered to the load must be scaled by the factor $(R_D - R_s)/R_D$, where R_D is the magnitude of the diode negative resistance ($R_D = 1\ \Omega$ for the cases in Table II).

It should be remarked that the maximum RF power given in Table II, 6.08 W, is not necessarily the maximum power this device is capable of generating when matched to 1-Ω circuit resistance. To find the overall maximum P_{RF}, both J_{dc} and V_{RF} must be varied, whereas V_{RF} is fixed for

TABLE III
CW RESULTS FOR STRUCTURE 1 OF TABLE I
$f = 33.7$ GHz, $T = 500$ K

J_{dc} (kA/cm^2)	V_{RF} (V)	CM D (inch) θ (°C/W) P_{RF} (W)	CM R_c (Ω)	DM D (inch) θ (°C/W) P_{RF} (W)	DM R_c (Ω)	CR D (inch) θ (°C/W) P_{RF} (W)	CR R_c (Ω)	DR D (inch) θ (°C/W) P_{RF} (W)	DR R_c (Ω)
5.92	14.0	0.00392 25.9 2.77	1.00 (E)	0.00392 25.9 2.77	1.00 (E)	0.00392 25.9 2.77	1.00 (E)	0.00392 25.9 2.77	1.00 (E)
6.94	14.0	0.00427 19.2 4.17	1.00 (E)	0.00427 19.2 4.17	1.00 (E)	0.00427 19.2 4.17	1.00 (E)	0.00427 19.2 4.17	1.00 (E)
8.10	14.0	0.00364 21.67 3.02	1.63	0.00464 13.5 5.13	1.00 (E)	0.00464 13.5 5.13	1.00 (E)	0.00464 13.5 5.13	1.00 (E)
10.0	14.0	0.00277 30.12 1.82	3.33	0.00506 9.10 6.08	1.00 (E)	0.00504 9.11 6.04	1.01	0.00506 9.10 6.08	1.00 (E)
12.0	14.0	0.00212 42.1 0.89	5.56	0.005 7.53 5.03	1.00 (E)	0.00386 12.7 2.96	1.68	0.005 7.53 5.03	1.00 (E)

TABLE IV
LARGE-SIGNAL RESULTS FOR STRUCTURE 6 OF TABLE I
$f = 33.7$ GHz, $T = 500$ K, $R_c = 1$ Ω matching

J_{dc} (kA/cm^2)	$-G_D$ (s/cm^2)	B_D (s/cm^2)	D (inch)	V_{RF} (V)	V_{op} (V)	η (%)	P_{RF} (W)	P_{diss} (W)	θ_R (°C/W)
5.00	221.9	2584	0.00255	18.0	25.26	28.33	1.19	2.98	75.4
5.94	275.2	2533	0.00289	18.0	25.74	29.15	1.89	4.59	49.01
7.13	324.1	2468	0.00321	18.0	25.68	28.64	2.86	6.72	33.51
10.01	417.4	2302	0.00388	18.0	25.29	26.68	5.18	14.15	15.90
13.06	472.9	2120	0.00445	18.0	24.62	23.82	7.68	24.43	9.21
15.23	466.1	1993	0.00468	18.0	23.86	20.78	8.40	32.03	7.02
16.00	421.3	1957	0.00456	18.0	23.23	18.38	7.17	31.85	7.07
20.10	534.5	1612	0.00605	17.0	23.49	16.36	14.32	73.22	3.07

the simulations of Table II. Reducing V_{RF} often allows operation at higher current densities with higher resulting P_{RF}, since reducing V_{RF} tends to increase the device area needed to match to 1 Ω. V_{RF} was varied for some cases presented in this paper, however, even for those cases an exhaustive search was not completed since the primary objective was to compare different structures, not to determine the maximum power generation capability of each structure.

It is not always possible to achieve the thermal resistance values given in Table II. Table III presents estimates of the maximum CW power obtainable at various current densities using different heat sink materials and diode geometries. The equations used to calculate the thermal resistance of the diode-heat sink combination are given in [7], [8]. In Table III, CM denotes copper heat sink and single mesa geometry; DM denotes diamond heat sink and single mesa geometry; CR denotes copper heat sink and ring geometry; and DR denotes diamond heat sink and ring geometry. In the thermal-resistance equations, it is assumed that improvement by the factor 0.55 of the spreading resistance term is achievable by using the ring geometry instead of a single-mesa structure. This could also be achieved by using four mesas with equivalent area.

For each case in Table III, the value of circuit resistance needed to match the diode R_c is given. In practice, it would be difficult to match the diode much below 1.0 Ω so that for the cases in Table III where the diode becomes thermally limited for $R_c < 1.0$ Ω, the data for $R_c = 1.0$ Ω is given. An "E" is appended with these cases to indicate that the diode is electronically limited before it is thermally limited due to matching considerations.

Table IV presents the large-signal results versus bias current density for structure 6 of Table I, which is the structure for which maximum efficiency was obtained at 33.7 GHz. In Table IV, P_{RF} is again the power that would be obtained if the diode is matched to 1-Ω circuit resistance. Table V gives the optimum expected CW performance of this device, taking into account the thermal resistance expressions and restricting the maximum device temperature rise from ambient to 225°C, while also requiring that $R_c \geq 1.0$ Ω.

Comparison of Tables II and IV shows that, if the two devices are matched to 1-Ω circuit resistance, the starting

TABLE V
CW RESULTS FOR STRUCTURE 6 OF TABLE I
$f = 33.7$ GHz, $T = 500$ K

J_{dc} (kA/cm^2)	V_{RF} (V)	CM D (inch) θ (°C/W) P_{RF} (W)	CM R_c (Ω)	DM D (inch) θ (°C/W) P_{RF} (W)	DM R_c (Ω)	CR D (inch) θ (°C/W) P_{RF} (W)	CR R_c (Ω)	DR D (inch) θ (°C/W) P_{RF} (W)	DR R_c (Ω)
5.00	18.0	0.00255 75.4 1.19	1.00 (E)	0.00255 75.4 1.19	1.00 (E)	0.00255 75.4 1.19	1.00 (E)	0.00255 75.4 1.19	1.00 (E)
5.94	18.0	0.00289 49.01 1.89	1.00 (E)	0.00289 49.01 1.89	1.00 (E)	0.00289 49.01 1.89	1.00 (E)	0.00289 49.01 1.89	1.00 (E)
7.13	18.0	0.00321 33.51 2.86	1.00 (E)	0.00321 33.51 2.86	1.00 (E)	0.00321 33.51 2.86	1.00 (E)	0.00321 33.51 2.86	1.00 (E)
10.01	18.0	0.002939 27.66 2.96	1.743	0.00388 15.90 5.18	1.00 (E)	0.00388 15.90 5.18	1.00 (E)	0.00388 15.90 5.18	1.00 (E)
13.06	18.0	0.00198 46.09 1.53	5.02	0.00445 9.21 7.68	1.00 (E)	0.00360 13.94 5.04	1.52	0.00445 9.21 7.68	1.00 (E)
15.23	18.0	0.00156 63.15 0.934	8.99	0.00468 7.02 8.40	1.00 (E)	0.00284 19.10 3.09	2.72	0.00468 7.02 8.40	1.00 (E)
16.00	18.0	0.00150 65.16 0.777	9.254	0.0045 7.24 7.00	1.028	0.002726 19.71 2.57	2.80	0.00456 7.07 7.17	1.00 (E)
20.10	17.0	0.000913 135 0.326	43.92	0.00274 14.99 2.94	4.87	0.00166 40.81 1.08	13.26	0.00498 4.53 9.70	1.48

TABLE VI
OPTIMUM LARGE-SIGNAL RESULTS AT 44 GHZ FOR DIFFERENT DOPING PROFILE PARAMETERS USING THE ENERGY-MOMENTUM SIMULATION
$N_A = 3.25\times10^{16}$, $N_D = 6.5\times10^{15}$, $T = 500$ K

Case No.	ℓ_p (μm)	ℓ_n (μm)	w (μm)	Q_p (10^{12} cm^{-2})	Q_n (10^{12} cm^{-2})	V_{RF} (V)	V_{op} (V)	J_{dc} (kA/cm^2)	η (%)	Y_D (s/cm^2)	P_{RF} (W/cm^2)	P_{RF} (1 Ω matching) (W)	P_{diss} (1 Ω matching) (W)
1	0.40	0.37	0.94	2.05	2.75	14.0	25.45	9.92	18.91	-487.2 +j2979	4.774 x 10^4	2.55	10.95
2	0.40	0.23	0.80	2.05	2.75	13.5	23.46	10.22	20.97	-551.7 +j3413	5.028 x 10^4	2.32	8.75
3	0.40	0.17	0.74	2.05	2.75	13.0	22.87	9.97	21.38	-576.9 +j3686	4.875 x 10^4	2.02	7.43
4	0.40	0.13	0.70	2.05	2.75	11.5	22.46	9.80	19.17	-637.9 +j3863	4.219 x 10^4	1.76	7.40
5	0.40	0.17	0.74	2.26	2.12	16.0	23.25	10.14	25.53	-470.2 +j3817	6.019 x 10^4	1.91	5.58
6	0.40	0.17	0.74	1.96	1.84	16.5	23.67	10.16	25.61	-452.6 +j3786	6.160 x 10^4	1.92	5.57
7	0.40	0.17	0.74	1.42	1.33	17.5	23.87	9.89	24.84	-383.1 +j3763	5.866 x 10^4	1.57	4.75

structure (number 1 of Table I) yields more RF power at lower current densities, whereas at higher current densities the optimized structure (number 6 of Table I) yields more power. *Structure* 1 *yields more power at low current densities because it is longer, which reduces the diode susceptance* B_D. *Since the area* A *needed to match the device to* $R_c = 1$ Ω *is given by*

$$A = \frac{|G_D|}{G_D^2 + B_D^2} \text{ cm}^2 \qquad (1)$$

a reduction in B_D yields a larger area A and hence more power. Here G_D, B_D are the device conductance and susceptance in s/cm^2. At higher current densities, the efficiency of structure 1 drops more rapidly than for structure 6, so that overall the highest power is generated by structure 6. Examining Tables III and V shows that, under CW conditions, structure 6 can generate more power provided diamond heat sinking is used.

III. RESULTS AT 44 GHZ

Table VI presents the optimum large-signal results obtained at $f = 44$ GHz, $T = 500$ K, and $J_{dc} \approx 10$ kA/cm^2. For case 1, the starting profile, the efficiency is lowest; however, matching the device to 1-Ω circuit resistance

TABLE VII
LARGE-SIGNAL RESULTS FOR STRUCTURE 1 OF TABLE VI
$f = 44$ GHz, $T = 500$ K, $R_c = 1\ \Omega$ matching

J_{dc} (kA/cm^2)	$-G_D$ (s/cm^2)	B_D (s/cm^2)	D (inch)	V_{RF} (V)	V_{op} (V)	η (%)	P_{RF} (W)	P_{diss} (W)	θ_R (°C/W)
10.0	543.0	2972	0.00342	13.0	25.87	17.9	2.73	12.64	17.8
11.8	626.3	2881	0.00377	13.0	25.84	17.27	3.81	18.26	12.32
14.3	718.3	2752	0.00419	13.0	25.77	16.46	5.94	26.09	8.62
16.0	738.9	2646	0.00440	13.0	25.42	15.33	6.11	33.70	6.68
18.0	740.4	2516	0.00461	13.0	25.00	13.90	6.74	41.71	5.39

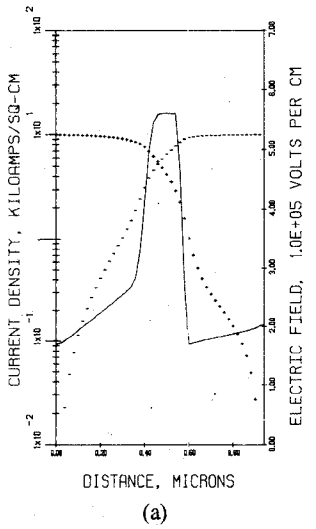

(a)

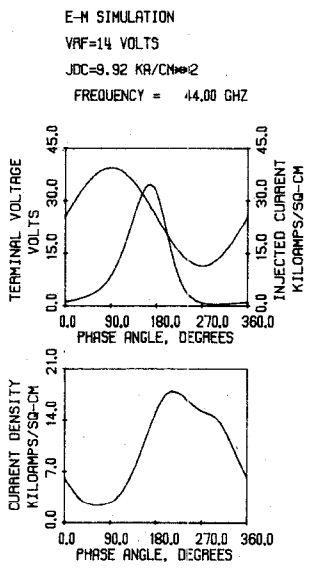

(b)

Fig. 5. (a) DC solution for case 1 of Table II ($T = 500$ K, $J_{dc} = 10$ kA/cm^2, $V_{dc} = 25.3$ V) and (b) most efficient large-signal solution for this case ($f = 44$ GHz, $V_{RF} = 14.0$ V, $J_{dc} = 9.92$ kA/cm^2, $T = 500$ K, $\eta = 18.91$ percent).

using (1) for the area yields the maximum RF power. In cases 2–4 of Table VI, the n drift length is progressively shortened and the efficiency is found to peak for the value $l_n = 0.17\ \mu$m. Variation of l_p was found not to increase the efficiency. For cases 5–7, the doping spikes Q_n and Q_p were reduced so that the electric field level in the drift regions was increased. Although case 6 resulted in the highest efficiency, case 5 was used as the optimum-efficiency profile since the difference between the two efficiencies was less than 0.1 percent and more data were already available for case 5.

Fig. 5(a) shows the dc solution at $T = 500$ K, $J_{dc} = 10$ kA/cm^2 for the starting profile of case 1 in Table VI, and Fig. 5 (b) shows the terminal waveforms for the most efficient RF solution obtained for this structure. From Fig. 5(a) it is seen that the electric field is higher in the p drift region than the n drift region for this device, so that the field will collapse on the n side first under large RF voltage swing, unlike the 33-GHz profile where the field on the p side reached a low value. Also, the field on the n side is increasing due to space charge, so that the "knee" of the curve goes to zero while the field in the remainder of the n drift region stays relatively high. Thus, it is anticipated that the velocity modulation effect will be less pronounced for this structure, and comparison of Figs. 5(b) and 2(b) shows that the dip and subsequent peak of induced current at 270° is much reduced in Fig. 5(b).

Table VII presents the large-signal results versus bias current density obtained for this structure at 44 GHz, and the power obtained by matching to 1-Ω circuit resistance is given. In Table VIII, the maximum expected CW powers obtainable using the thermal resistance expressions for the various cases described earlier are given. Also, for each case the required circuit resistance R_c is given.

Fig. 6(a) shows the dc solution at $T = 500$ K, $J_{dc} = 10$ kA/cm^2 for the optimized structure of case 5 in Table VI and Fig. 6(b) shows the terminal waveforms for the most efficient large-signal solution obtained for this structure with $\eta = 25.53$ percent. Fig. 6(a) shows that the best efficiency is obtained if the electric field at the edges of the high-field regions is raised to approximately 2.5×10^5 V/cm. Since the electric field on the p side is now lower than the field on the n side, it is expected that velocity modulation of holes will be important for this structure. The induced current waveform in Fig. 6(b) bears this out, since the dip and subsequent peak at 270° is now more pronounced.

Table IX presents the optimum large-signal results versus bias current density for structure 5 of Table VI, and the powers obtainable by matching to 1-Ω circuit resistance. Table X presents the expected CW powers obtainable

TABLE VIII
CW RESULTS FOR STRUCTURE 1 OF TABLE VI
$f = 44$ GHz, $T = 500$ K

J_{dc} (kA/cm^2)	V_{RF} (V)	CM D (inch) θ (°C/W) P_{RF} (W)	CM R_c (Ω)	DM D (inch) θ (°C/W) P_{RF} (W)	DM R_c (Ω)	CR D (inch) θ (°C/W) P_{RF} (W)	CR R_c (Ω)	DR D (inch) θ (°C/W) P_{RF} (W)	DR R_c (Ω)
10.0	13.0	0.00245 35.03 1.39	1.948	0.00342 17.8 2.73	1.00 (E)	0.00342 17.8 2.73	1.00 (E)	0.00342 17.8 2.73	1.00 (E)
11.8	13.0	0.00190 48.31 0.972	3.937	0.00377 12.32 3.81	1.00 (E)	0.00346 14.61 3.21	1.187	0.00377 12.32 3.81	1.00 (E)
14.3	13.0	0.00142 71.32 0.621	8.69	0.00419 8.62 5.94	1.00 (E)	0.00258 21.57 2.05	2.632	0.00419 8.62 5.94	1.00 (E)
16.0	13.0	0.001183 92.02 0.443	13.80	0.00355 10.22 3.98	1.533	0.00215 27.84 1.46	4.179	0.00440 6.68 6.11	1.00 (E)
18.0	13.0	0.00096 124.2 0.293	23.06	0.00288 13.8 2.63	2.562	0.001746 37.56 0.96	6.971	0.00461 5.39 6.74	1.00 (E)

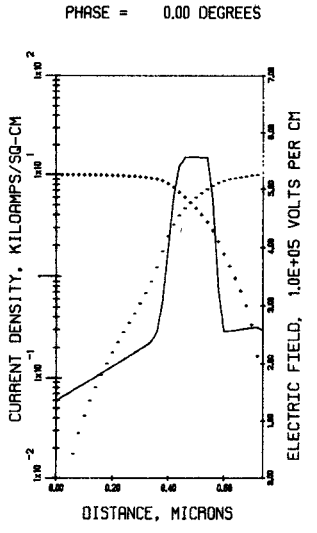

(a)

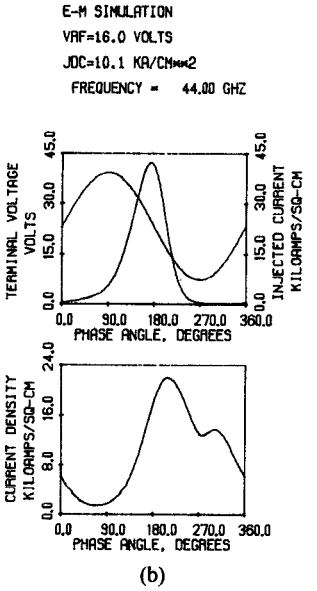

(b)

Fig. 6. (a) DC solution for case 5 of Table 2 ($T = 500$ K, $J_{dc} = 10$ kA/cm^2, $V_{dc} = 21.6$ V) and (b) most efficient large-signal solution for this case ($f = 44$ GHz, $V_{RF} = 16.0$ V, $J_{dc} = 10.14$ kA/cm^2, $T = 500$ K, $\eta = 25.53$ percent).

taking into account the thermal resistance expressions described previously.

Comparison of Tables VII and IX shows that the starting structure, number 1, generates more power than structure 5 at the same current density value; however, the dissipated power is larger for structure 1 and the required thermal resistance θ_R is lower. When the two devices are compared for approximately the same levels of dissipated power and θ_R, for example, taking $J_{dc} = 11.8$ kA/cm^2 for structure 1 and $J_{dc} = 18$ kA/cm^2 for structure 5, it is found that structure 5 generates more power (4.94 versus 3.81 W for structure 1). For pulsed applications where thermal considerations are not important, structure 1 may be preferred since a larger diode area may be used at a given bias current and circuit resistance level, resulting in higher power.

Comparison of Tables VIII and X shows that the optimized structure, number 5, can generate more power for CW operation, except for the case of a diamond heat sink and single-mesa structure. However, for this case the required thermal resistance is lower for structure 1, 8.62 versus 10.58 °C/W, due to the higher dissipated power.

IV. CONCLUSIONS

Double-read GaAs IMPATT doping profiles were optimized for maximum efficiency with respect to drift region lengths and integrated charge in the doping spikes at 33.7 and 44 GHz. For both frequencies, the best efficiency is obtained for electron drift region lengths significantly shorter than the values predicted by conventional IMPATT theory. These shorter structures are preferred for CW operation due to their less stringent thermal limitations, whereas the longer structures can deliver more power to a fixed circuit resistance under pulsed conditions where thermal limitations are not important. *The optimum electric field level at the edges of the high-field regions was found to be in the* 2.5 *to* 2.8×10^5 *V/cm range for the case where the fields on both sides are approximately equal.*

It is extremely important to emphasize that the power which can be generated from these devices depends on the

TABLE IX
LARGE-SIGNAL RESULTS FOR STRUCTURE 5 OF TABLE VI
$f = 44$ GHz, $T = 500$ K, $R_c = 1\ \Omega$ matching

J_{dc} (kA/cm^2)	$-G_D$ (s/cm^2)	B_D (s/cm^2)	D (inch)	V_{RF} (V)	V_{op} (V)	η (%)	P_{RF} (W)	P_{diss} (W)	θ_R (°C/W)
5.90	321.1	3961	0.002	14.5	23.36	24.70	0.69	2.11	106.5
7.83	427.6	3877	0.00236	14.5	23.45	24.33	1.26	3.90	57.74
10.14	470.2	3817	0.00251	16.0	23.25	25.53	1.91	5.58	40.32
12.25	558.9	3719	0.00279	16.0	23.24	25.14	2.83	8.41	26.75
14.76	626.3	3598	0.00304	16.0	22.90	23.72	3.76	12.17	18.49
16.93	680.7	3488	0.00326	16.0	22.70	22.70	4.70	16.01	14.05
18.0	688	3433	0.00333	16.0	22.10	21.78	4.94	17.39	12.94
19.14	738	3350	0.00352	15.75	22.50	21.25	5.74	21.27	10.58
23.64	845	3050	0.00408	15.25	22.2	18.67	8.28	35.99	6.25
25.06	851	2970	0.00419	15.25	22.2	17.86	8.83	40.77	5.25

TABLE X
CW RESULTS FOR STRUCTURE 5 OF TABLE VI
$f = 44$ GHz, $T = 500$ K

J_{dc} (kA/cm^2)	V_{RF} (V)	CM D (inch) / θ (°C/W) / P_{RF} (W)	CM R_c (Ω)	DM D (inch) / θ (°C/W) / P_{RF} (W)	DM R_c (Ω)	CR D (inch) / θ (°C/W) / P_{RF} (W)	CR R_c (Ω)	DR D (inch) / θ (°C/W) / P_{RF} (W)	DR R_c (Ω)
5.90	14.5	0.002 / 106.5 / 0.69	1.00 (E)	0.002 / 106.5 / 0.69	1.00 (E)	0.002 / 106.5 / 0.69	1.00 (E)	0.002 / 106.5 / 0.69	1.00 (E)
7.83	14.5	0.00236 / 57.74 / 1.26	1.00 (E)	0.00236 / 57.74 / 1.26	1.00 (E)	0.00236 / 57.74 / 1.26	1.00 (E)	0.00236 / 57.74 / 1.26	1.00 (E)
10.14	16.0	0.00251 / 40.32 / 1.91	1.00 (E)	0.00251 / 40.32 / 1.91	1.00 (E)	0.00251 / 40.32 / 1.91	1.00 (E)	0.00251 / 40.32 / 1.91	1.00 (E)
12.25	16.0	0.002421 / 35.54 / 2.125	1.328	0.00279 / 26.75 / 2.83	1.00 (E)	0.00279 / 26.75 / 2.83	1.00 (E)	0.00279 / 26.75 / 2.83	1.00 (E)
14.76	16.0	0.001858 / 49.86 / 1.403	2.677	0.00304 / 18.49 / 3.76	1.00 (E)	0.00304 / 18.49 / 3.76	1.00 (E)	0.00304 / 18.49 / 3.76	1.00 (E)
16.93	16.0	0.001503 / 66.11 / 0.997	4.704	0.00326 / 14.05 / 4.70	1.00 (E)	0.00273 / 19.99 / 3.298	1.43	0.00326 / 14.05 / 4.70	1.00 (E)
18.0	16.0	0.001378 / 73.92 / 0.8473	5.83	0.00333 / 12.94 / 4.94	1.00 (E)	0.002505 / 22.36 / 2.801	1.76	0.00333 / 12.94 / 4.94	1.00 (E)
19.14	15.75	0.001230 / 86.47 / 0.7021	8.18	0.00352 / 10.58 / 5.74	1.00 (E)	0.002237 / 26.16 / 2.321	2.47	0.00352 / 10.58 / 5.74	1.00 (E)
23.64	15.25	0.000808 / 158.7 / 0.3254	25.44	0.00243 / 17.64 / 2.929	2.83	0.001470 / 48.01 / 1.076	7.70	0.00408 / 6.25 / 8.28	1.00 (E)
25.06	15.25	0.000711 / 192.8 / 0.2536	34.82	0.00213 / 21.42 / 2.282	3.87	0.001293 / 58.33 / 0.8384	10.53	0.00388 / 6.48 / 7.546	1.17

actual circuit resistance, series resistance, and thermal resistance which can be achieved. The power levels predicted here are based on certain assumptions relative to these values and may be somewhat different in a particular experimental situation. However, when these values are known, it is believed that the data provided here will be extremely useful in the design of these devices and the prediction of their performance.

REFERENCES

[1] M. G. Alderstein and E. L. Moore, "Microwave properties of GaAs IMPATT diodes at 33 GHz," in *Proc. Eighth Biennial Cornell Electrical Engineering Conf.*, Aug. 1981, pp. 375–384.

[2] L. H. Holway, Jr., and S. L. Chu, "Broad-band characteristics of EHF IMPATT diodes," *IEEE Trans. Microwave Theory Tech.*, vol. MTT-30, pp. 1933–1939, Nov. 1982.

[3] R. Blumgold, private communication.

[4] R. K. Mains, G. I. Haddad, and P. A. Blakey, "Simulation of GaAs IMPATT diodes including energy and velocity transport equations,"

IEEE Trans. Electron Devices, vol. ED-30, pp. 1327–1338, Oct. 1983.
[5] D. Masse, G. Chu, K. Johnson, and M. Adlerstein, "High power GaAs millimeter wave IMPATT diodes," *Microwave J.*, vol. 22, pp. 103–105, June 1979.
[6] R. K. Mains, M. El-Gabaly, G. I. Haddad, and J. P. Sun, "Comparison of theoretical and experiment results for millimeter-wave GaAs IMPATTS," *IEEE Trans. Electron Devices*, vol. ED-31, no. 9, pp. 1273–1279, Sept. 1984.
[7] R. K. Mains and G. I. Haddad, "Properties and capabilities of millimeter-wave IMPATT diodes," in *Infrared and Millimeter Waves*, K. J. Button, Ed., vol. 10. New York: Academic, in press.
[8] R. K. Mains and G. I. Haddad, "Capabilities and pontential of millimeter-wave IMPATT devices," Electron Physics Laboratory, Univer. Michigan, Ann Arbor, Tech. Rep. AFWAL-TR-82-1141, Nov. 1982.

Moustafa A. El-Gabaly (S'70–M'74–SM'81) received the B.Sc. degree in electrical engineering and the B.Sc. degree in mathematics from the University of Cairo, Egypt, in 1965 and 1969, respectively. He received the Ph.D. degree in electrical engineering from the University of Alberta, Canada, in 1974.

During 1974 and 1975, he was with AGT, Canada, as a Design Microwave Systems Engineer. In 1976, he joined the faculty of the University of Kuwait, where he now an Associate Professor of Electrical Engineering. He also serves as a technical consultant at Kuwait Institute of Scientific Research. During the summers of 1977 to 1980, he was a Visiting Research Scientist at the Electron Physics Laboratory, the University of Michigan, Ann Arbor. Since April 1983, he has been a Visiting Associate Professor in the Department of Electrical and Computer Engineering, the University of Michigan. His research area includes microwave solid-state devices, photovoltaic energy conversion, and photoelectronic properties of crystalline and amorphous semiconductors.

Dr. El-Gabaly received the Government of Alberta Fellowship and the National Research Council of Canada Fellowship in 1972 and 1973, respectively. He is a Professional Engineer, registered in the Province of Alberta, Canada, and is a member of the Interantional Solar Energy Society (ISES).

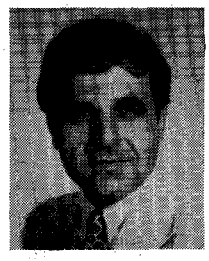

George I. Haddad (S'57–M'61–SM'66–F'72) was born in Aindara, Lebanon, on April 7, 1935. He received the B.S.E., M.S.E., and Ph.D. degrees in electrical engineering in 1956, 1958, and 1963, respectively, from the University of Michigan, Ann Arbor.

From 1957 to 1958 he was associated with the Engineering Research Institute of the University of Michigan, where he was engaged in research of electromagnetic accelerators. In 1958 he joined the Electron Physics Laboratory, University of Michigan, where he has been engaged in research of masers, parametric amplifiers, detectors, electron-beam devices, and microwave solid-state devices. He held a University of Michigan Research Institute Fellowship for the academic year of 1958–1959 and a sponsored fellowship for the spring semester of 1959–1960. He served successively as Instructor, Assistant Professor, and Associate Professor in the Department of Electrical Engineering from 1960 to 1969. He is presently a Professor and Chairman of the Department of Electrical and Computer Engineering.

Dr. Haddad received the 1970 Curtis W. McGraw Research Award of the American Society of Engineering Education for outstanding achievements as an Engineering Teacher. He is member of Eta Kappa Nu, Sigma Xi, Phi Kappa Phi, the American Physical Society, and the American Society for Engineering Education.

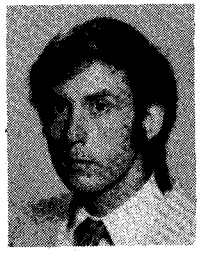

Richard K. Mains (S'79–M'79) was born in Chicago, IL, on March 28, 1950. He received the M.Sc. degree in electrical engineering in 1974 from Ohio State University, Columbus, and the Ph.D. degree in electrical engineering in 1979 from the University of Michigan, Ann Arbor.

At present, he is an assistant Research Scientist in the Electron Physics Laboratory, the University of Michigan.